Communication

Design, Synthesis and Antiproliferative Evaluation of Glucose 6″-OH Modified Open-Chain Analogues of Ipomoeassin F

Arman Khosravi , Precious Nnamdi , Alexa May , Kelsey Slattery , Robert E. Sammelson , Wei Q. Shi *

Posted Date: 31 October 2024

doi: 10.20944/preprints202410.2501.v1

Keywords: Ipomoeassin F; Resin Glycosides; Ring-Opened Analogues; Cytotoxicity; Sec61 Translocon

Communication

Design, Synthesis and Antiproliferative Evaluation of Glucose 6"-OH Modified Open-Chain Analogues of Ipomoeassin F

Arman Khosravi [1,†], Precious Nnamdi [1], Alexa May [2], Kelsey Slattery [1], Robert E. Sammelson [1] and Wei Q. Shi [1,*]

[1] Department of Chemistry, Ball State University, Muncie, Indiana 47306, United States
[2] Chemistry Department, Michigan State University, East Lansing, MI 48824, United States
* Correspondence: wqshi@bsu.edu (W.Q.S.)
† Current Address: Department of Chemistry, Purdue University, West Lafayette, IN 47907, USA

Abstract: Ipomoeassin F (Ipom-F) is a plant-derived macrocyclic resin glycoside that potently inhibits cancer cell growth through blockage of Sec61-mediated protein translocation at the endoplasmic reticulum. Recently, detailed structural information on how Ipom-F binds to Sec61α was obtained using Cryo-EM, which discovered that polar interactions between asparagine-300 (N300) in Sec61α and four oxygens in Ipom-F are crucial. One of the four oxygens is from the carbonyl group at C-4 of the fatty caid chain. In contrast, our previous structure–activity relationship (SAR) studies suggest that the carbonyl group is not essential. To resolve this discrepancy, we designed and synthesized two new open-chain analogues (**10** and **11**). **10** without the C-4 carbonyl had a dramatic activity loss, whereas **11** with an amide functional group was even more potent than Ipom-F. These new SAR data, in conjunction with some previous SAR information, imply two functional roles of the C-4 carbonyl: 1) to form H-bonds with N300; and 2) to regulate interactions of the fatty acid chain with membrane lipids. Impacts of these dual functions on antiproliferation depend on the overall structure of an Ipom-F derivative. Moreover, **11** can serve as a lead compound for developing future amino acid/peptide-modified analogues of Ipom-F with improved therapeutic properties.

Keywords: Ipomoeassin F; resin glycosides; ring-opened analogues; cytotoxicity; Sec61 translocon

1. Introduction

Natural products provide a rich source of molecular templates for development of novel pharmaceutical agents [1]. To date, six natural products have been discovered to block Sec61-mediated protein translocation [2,3], an essential cellular process for cell survival [4-6]. Therefore, they have attracted a great amount of research interest for their promising antibacterial, antiviral and antitumor activities. Structurally, these natural products can be classified into four categories: depsipeptides (cotransin (Figure 1) [7], coibamide A [8], and decatransin [9]), polyketides (mycolactone A/B (Figure 1) [10,11]), hybrid of depsipeptides and polyketides (apratoxins (Figure 1) [12,13]), and glycolipids (ipomoeassin F (Ipom-F, Figure 1) [14]). Despite distinct differences, all these molecules share a common structural feature, that is, a macrocyclic scaffold with different sizes ranging from 12-membered (mycolactone) to 30-membered ring (decatransin).

Among all the natural Sec61 inhibitors, Ipom-F is unique because it is to date the only one isolated from a plant as well as the only one containing carbohydrate fragments (Figure 1). Because of its high potency in inhibiting cancer cell growth in vitro [15], three independent total syntheses have been accomplished [16-18] since its discovery. Subsequent medicinal chemistry studies identified the pharmacophore of Ipom-F, that is, two α,β-unsaturated esters (cinnamate and tiglate, Figure 1) [19,20] and the disaccharide core [21]. Thanks to the optimized scalable synthesis [22], further biological and preclinical evaluations confirmed therapeutic potential of Ipom-F [23,24]. More intriguingly, it was discovered that unlike coibamide A [25], ring-opened analogues of Ipom-F could

 doi:10.20944/preprints202410.2501.v1

largely retain biological activities. For example, analogues **1–3** (Figure 2) are only 2–4-fold less potent than Ipom-F for inhibiting cancer cell proliferation [19,26].

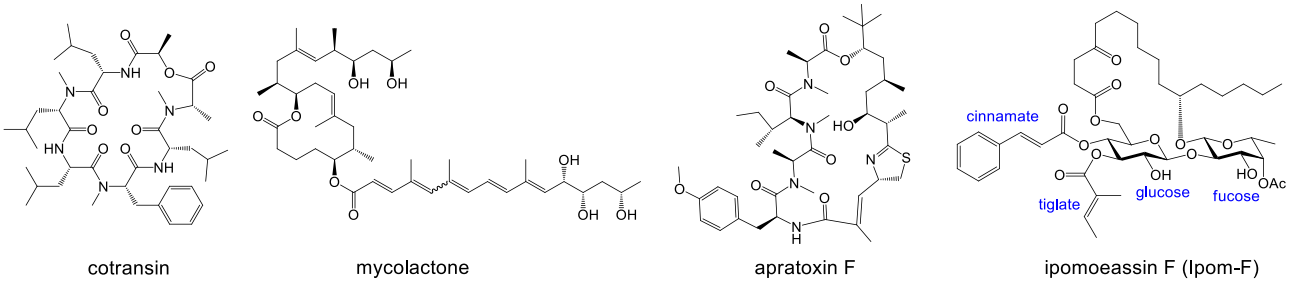

Figure 1. Structures of cotransin, mycolactone A/B, apratoxin F and ipomoeassin F (Ipom-F).

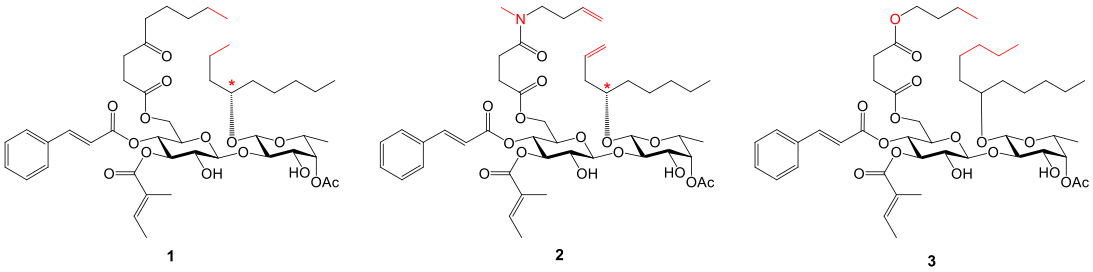

Figure 2. Structures of active open-chain analogues of Ipom-F (**1–3**). Major structural differences among the analogues are highlighted in red.

Very recently, detailed molecular interactions at the atomic level between Sec61α and the aforementioned natural products, except for coibamide A, have been revealed using the Cryo-EM technique [27], which shifts the research paradigm for developing Sec61α inhibitors from phenotype- to structure-based drug design. Among all the interactions, we are particularly attracted by polar interactions between asparagine-300 (N300) in Sec61α and heteroatoms (O/N) in the natural products (Figure 3, in orange). Mutational studies confirmed that substitution of asparagine with alanine (N300A) caused huge antiproliferative activity loss against HEK293 cells (> 1,000-fold and > 100,000-fold for Ipom-F and apratoxin F, respectively) [27], which demonstrates the indispensable role of such polar interactions.

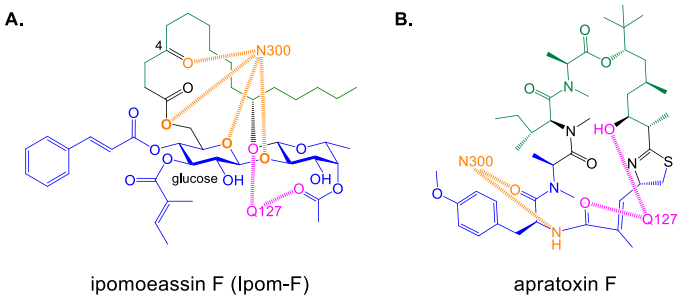

Figure 3. Maps for interactions between Sec61α and Ipom-F (A) or apratoxin F (B) obtained from cryo-EM. Main lipid-exposed portions are in green whereas channel-facing portions are in blue. Atoms/groups in orange and pink interact with N300 (Asn300) and Q127 (Gln127), respectively.

Although Cryo-EM clearly showed that the carbonyl group at C-4 of the fatty acid chain participated in the critical polar interactions of Ipom-F with N300 in Sec61α (Figure 3A), our structure–activity relationship (SAR) studies delivered contradictory information, that is, removal of the carbonyl group caused only marginal activity losses, no matter in the cyclic (**4** vs. Ipom-F, < 3-fold) [19] or acyclic (**5** vs. **6**, < 4-fold) [26] scaffold (Figure 4). To rationalize the discrepancy, we propose that the interactions between N300 and three oxygen atoms around the glucose moiety (Figure 3A, in orange and in bold) are sufficiently strong. The interaction between carbonyl and N300

 doi:10.20944/preprints202410.2501.v1

may make only negligible contribution to the binding of Ipom-F; therefore, we hypothesize that the carbonyl group at C-4 is dispensable. The primary goal of the work reported here is to test this hypothesis. In addition, we hope to further enrich our SAR knowledge on the open-chain system so that we may develop new analogues with better therapeutic properties.

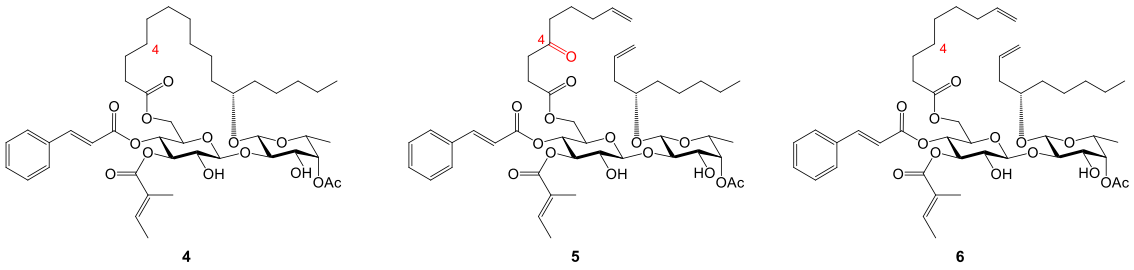

4 **5** **6**

Figure 4. Structures of analogues **5** with or **4** and **6** without a carbonyl group at the C-4 position (labelled in red) of the fatty acid chain.

2. Results and Discussion

*2.1. Design of Two New Open-Chain Analogues **10** and **11***

To date, compounds **1–3** (Figure 2) are the most potent open-chain analogues of Ipom-F. Among them, **3** can be more easily adapted to large-scale production [26]. Although mono-butyl succinate **7** (Figure 5), a building block for the synthesis of **3**, could be synthesized efficiently, it has limited stability for long-term storage at room temperature. To further streamline the synthesis of open-chain analogues and simultaneously test whether the carbonyl group at C-4 is essential, we designed analogue **10**, which can be synthesized from commercially available nonanoic acid **8** in replacement of **7**.

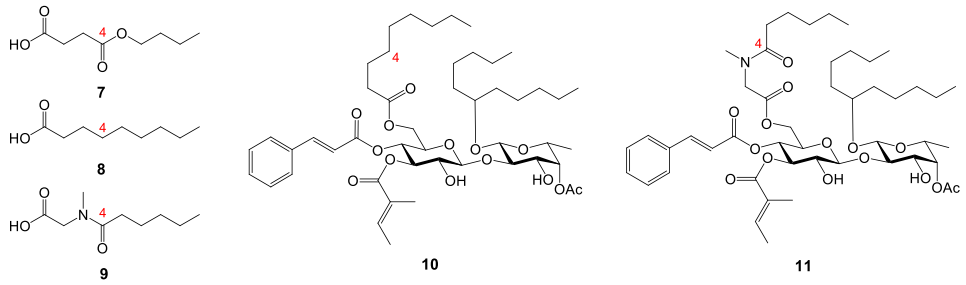

Figure 5. Structures of building blocks **7–9** and proposed analogues **10** and **11**.

Analogue **11** (Figure 5) was also designed for multiple purposes. First, it serves as an extra control compound with a carbonyl group at C-4. Secondly, the amide analogue **2** (IC_{50}: 41 nM) was 4-fold more potent than the ketone analogue **5** (IC_{50}: 170 nM) in the viability assay of HCT116 colon cancer cells [26]. More importantly, one of our goals in the future is to incorporate amino acids into the scaffold of Ipom-F because depsipeptides are the largest class of natural Sec61 inhibitors. Additionally, apratoxin F also contains a fragment of tetrapeptide and it is ~100-fold more potent than Ipom-F for inhibiting growth of HEK293 cells [27]. As a starting point, we proposed to replace **7** with *N*-hexanoyl-*N*-methylglycine (**9**) in the synthesis of **11** (Figure 5). Acid **9** could be prepared from commercially available *N*-methylglycine ethyl ester hydrochloride (see Supplementary Information 1).

 doi:10.20944/preprints202410.2501.v1

*2.2. Synthesis of New Open-Chain Analogues **10** and **11***

Synthesis of the target molecules started with D-glucose trichloroacetimidate donor **12** [22] and D-fucose acceptor **13** [26] (Scheme 1), which could be prepared by following previously established methods. It was observed that the first glycosylation reaction between **12** and **13** was temperature sensitive. When the temperature was above -30 °C, the acid-labile isopropylidene protecting group tended to break down, leading to a complex mixture of products and poor yield for the desired product [26]. When the temperature was below -65 °C, the reaction became sluggish. Around -50 °C seemed to be optimal for fast coupling of **12** with **13** while minimizing decomposition of isopropylidene. Afterwards, the remaining axial hydroxyl group was reacted with acetic anhydride to give the key disaccharide intermediate **14** in good yield (Scheme 1).

Because the final derivatization would occur at 6″-OH of the glucose moiety, we opted for early removal of the two levulinoyl (Lev) groups by hydrazine under buffered conditions to afford diol **15** in excellent yield (Scheme 1). Next, highly selective esterification of 3″-OH with tiglic acid was achieved to produce **16** efficiently, presumably because 2″-OH was conformationally shielded by the large TBS (*tert*-butyldimethylsilyl) group in the fucose moiety. Based on our previous investigation [22], 2″-OH was then protected by TES using triethylsilyl triflate (TESOTf). At this point, disaccharide **17** was ready for deprotection of isopropylidene by trifluoroacetic acid (TFA) to release 4″-OH and 6″-OH, leading to the formation of diol **18** in very good yield.

Subsequently, we explored selective esterification of 6″-OH in **18** with nonanoic acid **8,** followed by a second esterification with cinnamic acid to deliver the last intermediate **22** (Scheme 1). The advantage of this reaction sequence is that it doesn't require any protection/deprotection steps. In general, a primary alcohol is expected to be more reactive than a secondary alcohol; therefore, we thought coupling of **18** with **8** would primarily occur at 6″-OH. Unfortunately, we did not observe good selectivity for this particular substrate. In fact, it was not very surprising to us because we got poor selectivity before on a similar substrate [26]. More importantly, because byproducts generated from the reaction of **18** with **8** had similar polarity to that of the desired product, column purification of the desired product was challenging and the yield over two steps was usually 30–35%.

To improve the overall efficiency, we decided to introduce a bulky protecting group (triphenylmethyl, also known as trityl) to first block 6″-OH in diol **18** (Scheme 1). The yield for the reaction of trityl chloride with **18** was almost quantitative. Next, cinnamic acid reacted with 4″-OH using DCC (*N*,*N*′-dicyclohexylcarbodiimide) as the coupling reagent. Relatively weaker coupling reagents, such as EDC (1-ethyl-3-(3-dimethylaminopropyl)carbodiimide) and CMPI (2-chloro-1-methylpyridinium iodide), could not fully convert **19** to **20**, presumably because of the large steric hindrance caused by the enormous trityl group. After the trityl group was cleaved, the released 6″-OH was then coupled with **8** to give **22**, which could not be purified because it had almost the same R_f as **8**. Extra **8** was removed in the following step. Although this new route added two extra protection and deprotection steps, they were easy to perform and the yield for converting **18** to **22** increased to ~55%. Another advantage to this revised procedure is that different carboxylic acids could be introduced in the penultimate step, which makes future library assembly much more efficient. Finally, both TES and TBS groups were removed by TBAF (tetra-n-butylammonium fluoride) buffered with acetic acid to give the target molecule **10**.

Similarly, target molecule **11** was prepared in two steps from **21** and **9** (see Supplementary Information 1 for synthesis and characterization of **9**). Syntheses of the intermediate **23** and the final product **11** were straightforward. However, due to the coexistence of *cis-trans* amide bond rotamers, it was difficult to accurately interpret the NMR spectra for both **23** and **11**. Nevertheless, using both ^{1}H and ^{13}C NMR, we were able to estimate the ratio of the two rotamers in either **23** or **11** was about 3–3.5:1. The identity of the final product **21** was further confirmed by high resolution mass spectrometry (HRMS). The purity of **21** was analyzed by reverse-phase HPLC.

 doi:10.20944/preprints202410.2501.v1

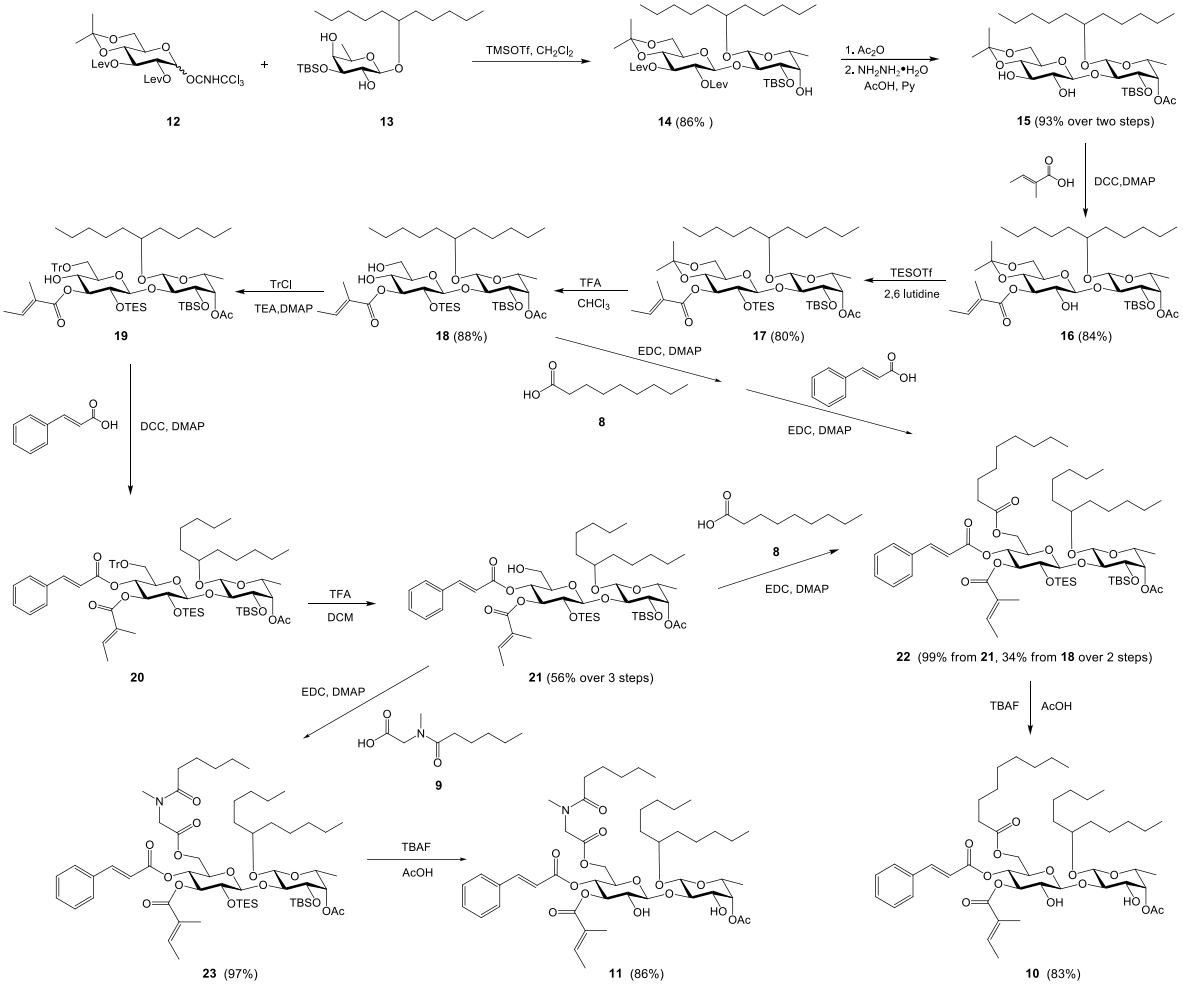

Scheme 1. Synthesis of the rationally designed, new open-chain analogues (**10** and **11**) of Ipom-F.

*2.3. Antiproliferative Activity of New Open-Chain Analogues **10** and **11***

With the two target molecules in hand, we evaluated their antiproliferative activity quantitatively using alamarBlue assay. MDA-MB-231 cells were used in the assay because this cell line was one of the cell lines that were most sensitive to Ipom-F in the NCI 60-cell line screen [20]. Ipom-F and analogue **3** were selected as positive controls and showed EC_{50}s (half-maximal effective concentrations) as 6.6 nM and 23.4 nM (Figure 6), respectively, which are consistent with the previously reported values [18,26]. To our surprise, analogue **10** was very inactive. Its EC_{50} was 444 nM, which is more than 65-fold less active than Ipom-F and ~19-fold less potent than 5-oxo analogue **3**. Even at 20 μM, **10** could inhibit only 60–70% cell growth. Therefore, we also used the software to estimate absolute IC_{50}s (half-maximal inhibitory concentrations) as indicated by a dashed line in the dose-response curve (Figure 6), which are 20.9 nM, 42.0 nM and 4787 nM for Ipom-F, **3** and **10**, respectively. According to the IC_{50}s, **10** is even ~230-fold less active than Ipom-F and over 110-fold less potent than analogue **3**. In contrast, the glycine-modified analogue **11** was very active and showed EC_{50} and absolute IC_{50} as 5.9 nM and 10.8 nM, respectively.

 doi:10.20944/preprints202410.2501.v1

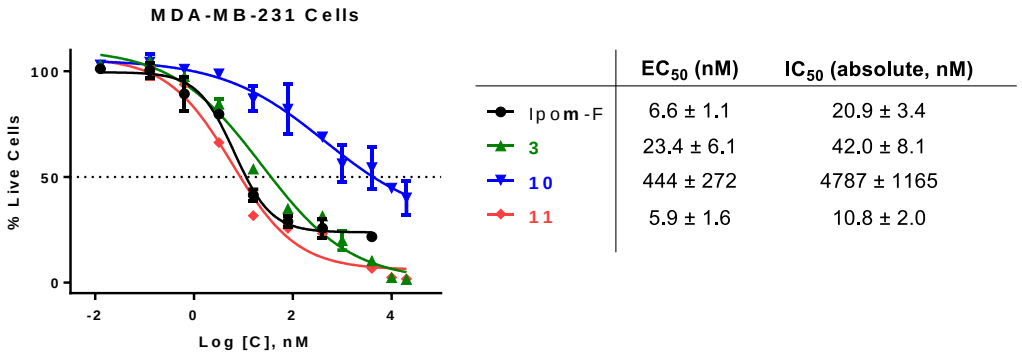

	EC_{50} (nM)	IC_{50} (absolute, nM)
Ipom-F	6.6 ± 1.1	20.9 ± 3.4
3	23.4 ± 6.1	42.0 ± 8.1
10	444 ± 272	4787 ± 1165
11	5.9 ± 1.6	10.8 ± 2.0

Figure 6. EC_{50}s and absolute IC_{50}s of Ipom-F and open-chain analogues **3**, **10** and **11** against MDA-MB-231 breast cancer cells. The data are derived from 2–3 independent assay experiments.

To confirm the above results from the quantitative assays, we also monitored changes in cell morphology and density at the end of the drug treatments before adding the alamarBlue dye (Figure 7). Figure 7a shows cell morphology and density for 0.5% DMSO, serving as a negative control. Significant changes in cell morphology and density for Ipom-F occurred at ~16 nM (Figure 7b–7d). It was of note that even at higher concentrations (≥ 80 nM) of Ipom-F, there were always some live cells as shown by cyan stars in Figure 7c and 7d, which matches with the IC_{50} curve that flattens out at 75–80% inhibition for Ipom-F (Figure 6). This suggests that the inhibition effect of Ipom-F is primarily cytostatic instead of cytotoxic. For analogue **3**, significant changes in cell morphology and density also occurred at ~16 nM (Figure 7e–7h). Unlike Ipom-F, however, very few cells could be seen in the elongated normal morphology at high concentrations (≥ 80 nM, Figure 7h), which suggests that **3** is likely cytotoxic when concentrations are high.

 doi:10.20944/preprints202410.2501.v1

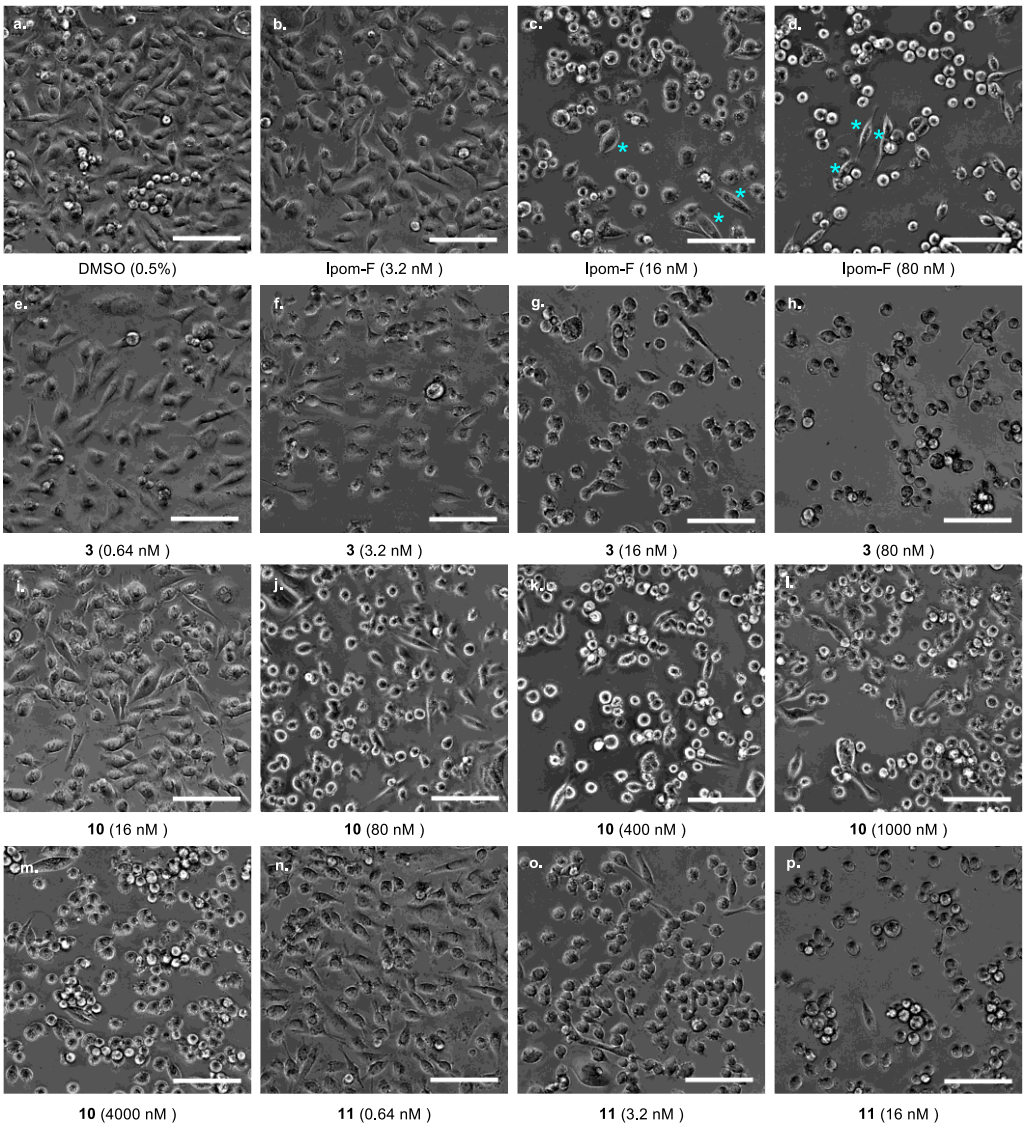

Figure 7. Cell morphology and density changes under treatments of Ipom-F or open-chain analogues (**3**, **10** and **11**) at different concentrations. Cyan stars in pictures c. and d. indicate live MDA-MB-231 cells. Scale bar = 100 μm.

When the cells were treated with analogue **10**, we appreciated significant cell morphology changes at 80 nM (Figure 7j) when compared to 16 nM (Figure 7i). However, we still saw live cells with the elongated normal morphology even up to 1 μM (Figure 7l). More importantly, compared to Ipom-F and **3**, cell density was significantly higher (Figure 7k–7m), even when the concentration of **10** reached its solubility limit, 20 μM. This suggests that cell growth arrest by **10** was temporary. Over time, the cells escaped from the arrest and continued to proliferate. Observations for cell morphology and density changes for analogue **11** largely mirrored what was observed for Ipom-F and **3** but at lower concentrations (0.64–16 nM, Figure 7n–7p), which proves that **11** is more potent. To conclude, the results from the qualitative analyses of cell morphology and density support the EC_{50}/IC_{50} values from the quantitative assays.

Analogues **1, 3** (Figure 2) and **10** (Figure 5) share great structural similarity. The major difference between them is that **1** and **3** have a carbonyl group at C-4, which is missing in analogue **10**. Given the significant activity loss for analogue **10** when compared to **1** (IC_{50}: 18.8 nM against MDA-MB-231 cells [19]) and **3**, it is clear that the carbonyl group at C-4 is essential in this case. Our rationale is that without the carbonyl group, the straight lipid chain in nonanoate can form tight packing with membrane lipids in the lateral gate, which may significantly distort molecular conformation of **10**, therefore weakening its binding to Sec61α. On the other hand, when compared to Ipom-F (Figure 1),

 doi:10.20944/preprints202410.2501.v1

analogue **4** (Figure 4) misses the C-4 carbonyl group but is still very active (IC_{50}: 16.1 nM against MDA-MB-231 cells) [19]. We think this can be attributed to the macrocyclic framework of analogue **4** that would restrict any major conformational changes. Moreover, the only structural difference between analogues **5** and **6** (Figure 4) is the presence or absence of the C-4 carbonyl group, but they have rather similar antiproliferative activity (IC_{50}: 59.1 nM and 205 nM, respectively, ~3.5-fold) against MDA-MB-231 cells [19,26]. Here, the flat distal alkene may prevent strong interactions between 8-nonenoate and membrane lipids, therefore helping retain the conformation for the most part. Putting all the information together, we believe that the carbonyl group at C-4 has two functional roles. The major role is to achieve balanced hydrophobic interactions with membrane lipids while minimizing conformational distortion. The minor role is to form polar interactions with N300 in Sce61α.

In support of our analyses above, analogue **11** with a carbonyl group at C-4 fully restored the antiproliferative activity. It is even more intriguing that **11** is the first open-chain analogue that showed potency superior to Ipom-F, albeit slightly. Besides the right conformation of **11**, it is likely that through resonance, the electron density on oxygen of the carbonyl group is enhanced, which strengthens its polar interaction (likely hydrogen bonding) with N300. This activity augment was also observed between analogues **2** and **5** (IC_{50}: 41 nM and 170 nM, respectively, against HCT116 colon cancer cells, and IC_{50}: 43 nM and 59 nM, respectively, against MDA-MB-231 cells) [26], but not in the cyclic system [28], which suggests that the ring-opened system might be better for harvesting polar interactions between N300 and Ipom-F derivatives. More importantly, **11** is the first amino acid-modified analogue of Ipom-F, which warrants further studies of new Ipom-F derivatives containing amino acids/peptides.

3. Materials and Methods

3.1. Chemical Synthesis General Methods

Unless otherwise stated, all commercially obtained reagents were used without further purification and all reactions were conducted under argon/nitrogen atmosphere. Reaction progress was monitored by TLC using silica gel F254 glass back plates with detection under UV lamp (254 nm) or charring with 5 % (v/v) H_2SO_4 (sulfuric acid) in EtOH (ethanol). Column chromatographic purifications were performed using silica gel (70 – 230 mesh) with a ratio that spanned from 100 to 50: 1 (w/w) between the silica gel and crude products. All ^{1}H NMR spectra were obtained in deuterated chloroform ($CDCl_3$), using chloroform ($CHCl_3$, δ = 7.26) or tetramethylsilane (TMS, δ = 0) as an internal reference. All ^{13}C NMR spectra were proton decoupled and obtained in $CDCl_3$ with $CHCl_3$ (δ = 77.16) as internal references. NMR data are reported in the form: chemical shifts (δ) in ppm, multiplicity, coupling constants (J) in Hz, and integrations. ^{1}H data are reported as though they were first order. Other 1D and 2D NMR spectra like ^{135}DEPT, COSY, HMQC, and HMBC were collected in addition to ^{1}H and ^{13}C for new compounds. High resolution mass spectrometry (HRMS) data were acquired by the Mass Spectrometry Lab at the University of Illinois Urbana-Champaign. Purity was analyzed using a Shimadzu HPLC with a dual wavelength UV detector set at 254 nm and 280 nm, a RESTEK Ultra reverse phase column (C18, 5 µm, 4.6x200 mm) and an isocratic mobile phase of acetonitrile in water.

3.1.1. Synthesis of Compound **14**

The fucoside diol acceptor **13** (1.10 g, 2.54 mmol), glucoside trichloroacetimidate donor **12** (1.57 g, 2.80 mmol, 1.1 equiv), and crushed activated 4Å molecular sieves (2.8 g) were suspended in 40 ml anhydrous CH_2Cl_2. The mixture was stirred under an argon atmosphere for ~30 min at room temperature and then cooled to −52 °C to −58 °C. To the cold reaction mixture was added TMSOTf (41 µl, 0.229 mmol, 0.09 equiv) via a syringe. The reaction was left to stir for 18 mins at this temperature and then quenched by addition of a few drops of TEA. The mixture was filtered through a pad of celite, and the filtrate was then concentrated. The resulting residue was purified by column

 doi:10.20944/preprints202410.2501.v1

chromatography (10:1→2:1 hexanes–EtOAc) to afford the product **14** as a yellow oil sticky oil (1.82 g, 86%). Its NMR data match with the literature-reported data [26].

3.1.2. Synthesis of Compound **15**

To an ice-cold solution of **14** (1.82 g, 2.19 mmol), TEA (2.44 ml, 17.52 mmol, 8 equiv), and DMAP (26.8 mg, 0.219 mmol, 0.1 equiv) in DCM (14 ml) was added Ac_2O (1.76 ml, 18.61 mmol, 8.5 equiv) dropwise and the reaction was warmed to room temperature overnight. At this point, TLC (Hex: EtOAc 3:1) showed the reaction was complete. Methanol was added to quench the reaction. DCM was added and the mixture was washed with 1N HCl (2x) followed by saturated $NaHCO_3$ wash. The aqueous layers were extracted with DCM twice and the combined organic layers were dried over Na_2SO_4. Rotary evaporation of the solvents yielded the crude product as a pale-yellow syrup (1.82 g 95%), which was moved to the next step without further purification.

To an ice-cold solution of the syrup obtained above (350.0 mg, 0.40 mmol) in DCM (5 ml) was added a buffer solution of hydrazine monohydrate (110 mg, 2.20 mmol, 5.5 equiv) in acetic acid (1.47 ml, 25.6 mmol, 64 equiv) and pyridine (2.20 ml, 68 equiv). The mixture was stirred at 0 °C for 30 minutes and then at room temperature for 1 hour. At this point, TLC showed the reaction was complete. The mixture was washed with 1M HCl (3x), followed by brine wash. All the aqueous layers were extracted twice by DCM and the combined organic layers were dried over Na_2SO_4. After solvent evaporation, the residue was purified by column chromatography (2:1, hexanes–EtOAc) to afford **15** as a white foam (265.0 mg, 98%): ^{1}H NMR (400 MHz, $CDCl_3$, δ_H) 4.98 (d, *J* = 3.3 Hz, 1H), 4.54 (d, *J* = 7.7 Hz, 1H), 4.29 (d, *J* = 7.4 Hz, 1H), 3.65–3.88 (m, 4H), 3.44–3.62 (m, 5H), 3.31 (t, *J* = 8.4 Hz, 1H), 3.20 (td, *J* = 9.9, 5.2 Hz, 1H), 3.01 (br s, 1H), 2.04 (s, 3H), 1.32–1.56 (m, 10H), 1.12–1.31 (m, 12H),1.05 (d, *J* = 6.4 Hz, 3H), 0.74–0.87 (m, 15H), 0.09 (s, 3H), 0.07 (s, 3H); ^{13}C NMR (100 MHz, $CDCl_3$, δ_C) 170.7 (C=O), 104.2 (O_2C), 101.1 (O_2CH), 99.7 (O_2CH), 79.8 (OCH), 79.0 (OCH), 76.5 (OCH), 73.3 (OCH), 72.9 (OCH), 72.6 (OCH), 72.5 (OCH), 68.6 (OCH), 68.2 (OCH), 62.2 (OCH_2), 34.0 (CH_2), 33.4 (CH_2), 32.1 (CH_2), 31.9 (CH_2), 29.0 (CH_3), 25.8 ($C(\underline{C}H_3)_3$), 24.8 (CH_2), 24.2 (CH_2), 22.5(9) (CH_2), 22.5(7) (CH_2), 20.8 (CH_3), 19.0 (CH_3), 17.8 ($Si\underline{C}(CH_3)_3$), 16.4 (CH_3), 14.1 (2xCH_3), -4.5 ($SiCH_3$), -4.7 ($SiCH_3$).

3.1.3. Synthesis of Compound **16**

To an ice-cold solution of **15** (230.0 mg, 0.334 mmol), DMAP (8.3 mg, 0.2 equiv) and tiglic acid (40.8 mg, 1.2 equiv) in DCM (5 ml) was added DCC (140.0 mg, 2.0 equiv). The reaction mixture was stirred overnight while warming up to room temperature. TLC showed the reaction was complete. Hexanes (5 mL) and ether (10 ml) were added, and the mixture was stirred for 20 more minutes. The resulting suspension was then filtered through a pad of celite. After solvent evaporation, the residue was purified by column chromatography (30:1→20:1, hexanes–EtOAc) to afford **16** as a white foam (217.0 mg, 84%): ^{1}H NMR (400 MHz, $CDCl_3$, δ_H) 6.80 (q, *J* = 7.1 Hz, 1H), 5.09 (t, *J* = 9.5 Hz, 1H), 5.00 (d, *J* = 3.3 Hz, 1H), 4.66 (d, *J* = 7.5 Hz, 1H), 4.30 (d, *J* = 7.5 Hz, 1H), 3.78–3.94 (m, 2H), 3.68–3.77 (m, 2H), 3.50–3.67 (m, 3H), 3.40–3.49 (m, 2H), 3.30 (td, *J* = 9.9, 5.1 Hz, 1H), 2.04 (s, 3H), 1.72–1.80 (m, 6H), 1.12–1.59 (m, 22H), 1.07 (d, *J* = 6.3 Hz, 3H), 0.74–0.91 (d, *J* = 11.2 Hz, 15H), 0.11 (s, 3H), 0.08 (s, 3H); ^{13}C NMR (100 MHz, $CDCl_3$, δ_C) 170.8 (C=O), 167.5 (C=O), 137.3 (=CH), 128.4 (=C), 104.4 (O_2C), 101.3 (O_2CH), 99.6 (O_2CH), 79.8 (OCH), 78.8 (OCH), 75.3 (OCH), 72.9 (OCH), 72.8 (OCH), 72.7 (OCH), 71.7 (OCH), 68.6 (OCH), 68.3 (OCH), 62.3 (OCH_2), 34.0 (CH_2), 33.4 (CH_2), 32.2 (CH_2), 31.9 (CH_2), 28.9 (CH_3), 25.8 ($C(\underline{C}H_3)_3$), 25.0 (CH_2), 24.8 (CH_2), 24.2 (CH_2), 22.6(5) (CH_2), 22.6(1) (CH_2), 20.9 (CH_3), 18.9 (CH_3), 17.8 ($Si\underline{C}(CH_3)_3$), 16.4 (CH_3), 14.3 (CH_3), 14.1 (CH_3), 12.1 (CH_3), -4.5(2) ($SiCH_3$), -4.5(8) ($SiCH_3$).

3.1.4. Synthesis of Compound **17**

To a solution of **16** (217.0 mg, 0.286 mmol) and 2,6 lutidine (153.0 mg, 5 equiv) in DCM (3.0 ml) at room temperature was added TESOTf (151.0 mg, 2.0 equiv). The mixture was stirred for one hour. At this point, TLC showed the reaction was complete. The mixture was washed with 1M HCl (2x), followed by brine wash. All the aqueous layers were extracted by DCM twice and the combined organic layers were dried over Na_2SO_4. After the solvents were removed by rotary evaporation, the

 doi:10.20944/preprints202410.2501.v1

residue was purified by column chromatography (30:1→20:1, hexanes–EtOAc) to afford **17** as a yellow sticky oil (200.1 mg, 80%): H NMR (400 MHz, $CDCl_3$, δ_H) 6.79 (qd, *J* = 7.0, 1.6 Hz, 1H), 5.00 (t, *J* = 9.3 Hz, 1H), 4.88–4.96 (m, 2H), 4.20 (d, *J* = 7.7 Hz, 1H), 3.87–4.01 (m, 2H), 3.81 (dd, *J* = 9.2, 3.6 Hz, 1H), 3.64 (t, *J* = 10.5 Hz, 1H), 3.57 (q, *J* = 6.4 Hz, 1H), 3.41–3.52 (m, 3H), 3.20 (td, *J* = 9.9, 5.2 Hz, 1H), 2.06 (s, 3H), 1.72–1.82 (m, 6H), 1.14–1.66 (m, 22H), 1.07 (d, *J* = 6.4 Hz, 3H), 0.78–0.96 (m, 24H), 0.40–0.63 (m, 6H), 0.11 (s, 3H), 0.05 (s, 3H); ^{13}C NMR (100 MHz, $CDCl_3$, δ_C) 170.9 (C=O), 166.8 (C=O), 137.0 (=CH), 128.7 (=C), 101.6 (O_2CH), 101.1 (O_2C), 99.3 (O_2CH), 82.0 (OCH), 74.9 (OCH), 74.5 (OCH), 74.4 (OCH), 74.0 (OCH), 73.4 (OCH), 72.5 (OCH), 68.8 (OCH), 67.2 (OCH), 62.6 (OCH_2), 34.6 (CH_2), 34.2 (CH_2), 32.4 (CH_2), 32.0 (CH_2), 29.0 (CH_3), 25.9 ($C(\underline{C}H_3)_3$), 25.2 (CH_2), 24.6 (CH_2), 23.1 (CH_2), 22.7 (CH_2), 21.0 (CH_3), 18.8 (CH_3), 17.7 ($Si\underline{C}(CH_3)_3$), 16.8 (CH_3), 14.4 (CH_3), 14.3 (CH_3), 14.1 (CH_3), 12.1 (CH_3), 6.9 ($3xSiCH_2\underline{C}H_3$), 5.0 ($3xSi\underline{C}H_2CH_3$), -4.1 ($SiCH_3$), -4.3 ($SiCH_3$).

3.1.5. Synthesis of Compound **18**

To an ice-cold solution of **17** (168.0 mg, 0.229 mmol) in $CHCl_3$ (3.00 ml) was added TFA (130 mg, 5 equiv). The mixture was stirred at 0 °C for two hours. At this point, TLC showed the reaction was complete. Water was added. The mixture was then extracted with DCM and washed with $NaHCO_3$. All the aqueous layers were extracted with DCM twice and the combined organic layers were dried over Na_2SO_4. After the solvents were removed by rotary evaporation, the residue was purified by column chromatography (6:1→4:1, hexanes–EtOAc) to afford **18** as a white foam (168.0 mg, 88%): ^1H NMR (400 MHz, $CDCl_3$, δ_H) 6.88 (q, *J* = 7.0 Hz, 1H), 4.85–4.99 (m, 3H), 4.21 (dd, *J* = 7.8, 1.9 Hz, 1H), 3.94 (td, *J* = 8.3, 1.9 Hz, 1H), 3.78–3.90 (m, 2H), 3.71 (dd, *J* = 12.2, 4.3 Hz, 1H), 3.41–3.63 (m, 4H), 3.25–3.35 (m, 1H), 2.93 (d, *J* = 5.4 Hz, 1H), 2.60 (s, 1H), 2.09 (s, 3H), 1.77–1.85 (m, 6H), 1.38–1.53 (m, 4H), 1.17–1.38 (m, 12H), 1.08 (d, *J* = 6.4 Hz, 3H), 0.76–0.95 (m, 24H), 0.45–0.63 (m, 6H), 0.11 (s, 3H), 0.07 (s, 3H); ^{13}C NMR (100 MHz, $CDCl_3$, δ_C) 171.1 (C=O), 168.8 (C=O), 138.4 (=CH), 128.3 (=C), 101.6 (O_2CH), 100.5 (O_2CH), 81.9 (OCH), 79.0 (OCH), 75.3 (OCH), 74.5 (OCH), 74.0 (OCH), 73.7 (OCH), 73.4 (OCH), 70.7 (OCH), 68.9 (OCH), 62.3 (OCH_2), 34.6 (CH_2), 34.2 (CH_2), 32.4 (CH_2), 32.0 (CH_2), 25.9 ($C(\underline{C}H_3)_3$), 25.2 (CH_2), 24.7 (CH_2), 22.9 (CH_2), 22.7 (CH_2), 21.1 (CH_3), 17.7 ($Si\underline{C}(CH_3)_3$), 16.8 (CH_3), 14.5 (CH_3), 14.3 (CH_3), 14.1 (CH_3), 12.1 (CH_3), 6.9 ($3xSiCH_2\underline{C}H_3$), 5.1 ($3xSi\underline{C}H_2CH_3$), -4.1 ($SiCH_3$), -4.3 ($SiCH_3$).

3.1.6. Synthesis of Compound **19**

To a solution of diol **18** (168.0 mg, 0.201 mmol), TEA (40.8 mg, 2.0 equiv) and DMAP (2.5 mg, 0.1 equiv) at room temperature was added trityl chloride (78.7 mg, 1.40 equiv). After the reaction mixture was stirred at room temperature overnight, TLC showed the reaction was complete. After solvent evaporation, the residue was purified by column chromatography (40:1→20:1, hexanes–EtOAc) to afford **19** as a white foam (214.0 mg, 99%). The successful installation of the trityl group was confirmed by a quick NMR check. No full NMR characterization was conducted.

3.1.7. Synthesis of Compound **20**

To an ice-cold solution of **19** (214.0 mg, 0.199 mmol), DMAP (4.9 mg, 0.2 equiv) and cinnamic acid (41 mg, 1.40 equiv) in DCM (4 ml) was added DCC (164.0 mg, 4.0 equiv). The mixture was stirred while warming up to room temperature overnight. At this point, TLC showed the reaction was complete. Hexanes (5 mL) and ether (10 ml) was added. The reaction mixture was stirred for another 20 minutes, and then filtered through a pad of celite. After the solvents were removed by rotary evaporation, the residue was purified by column chromatography (50:1→30:1, hexanes–EtOAc) to afford **20** as a white foam (189 mg, 79%). The presence of the cinnamate group was confirmed by a quick NMR check, but full NMR characterization was not conducted.

3.1.8. Synthesis of Compound **21**

To an ice-cold solution of **20** (189 mg, 0.156 mmol) in DCM (2.00 ml) was added TFA (89.0 mg, 5 equiv). The mixture was stirred at 0 °C for 30 minutes. At this point, TLC showed the reaction was complete. The mixture was washed with saturated $NaHCO_3$, followed by brine wash. All the aqueous

 doi:10.20944/preprints202410.2501.v1

layers were extracted twice with DCM and the combined organic layers were dried over Na_2SO_4. After solvents were evaporated, the residue was purified by column chromatography (30:1→5:1, hexanes–EtOAc) to afford **21** as a white foam (107 mg, 71%): ^{1}H NMR (400 MHz, $CDCl_3$, δ_H) 7.60 (d, *J* = 16.0 Hz, 1H), 7.42–7.52 (m, 2H), 7.29–7.40 (m, 3H), 6.79 (qd, *J* = 7.0, 1.6 Hz, 1H), 6.31 (d, *J* = 16.0Hz, 1H), 5.26 (t, *J* = 9.5 Hz, 1H), 4.96–5.09 (m, 3H), 4.26 (d, *J* = 7.6 Hz, 1H), 3.99 (dd, *J* = 9.1, 7.6 Hz, 1H), 3.87 (dd, *J* = 9.1, 3.7 Hz, 1H), 3.67–3.77 (m, 1H), 3.49–3.66 (m, 5H), 2.12 (s, 3H), 1.68–1.77 (m, 6H), 1.19–1.64 (m, 16H), 1.13 (d, *J* = 6.4 Hz, 3H), 0.80–1.00 (m, 24H), 0.46–0.66 (m, *6*H), 0.18 (s, 3H), 0.11 (s, 3H); ^{13}C NMR (100 MHz, $CDCl_3$, δ_C) 171.0 (C=O), 167.0 (C=O), 166.0 (C=O), 146.2 (=CH), 138.2 (=CH), 134.2 (=C), 130.6 (=CH), 129.0 (2x=CH), 128.3 (2x=CH), 128.2 (=C), 116.9 (=CH), 101.4 (O_2CH), 100.8 (O_2CH), 81.8 (OCH), 75.0 (OCH), 74.5 (OCH), 74.4 (OCH), 74.0(8) (OCH), 74.0(4) (OCH), 73.5 (OCH), 69.8 (OCH), 68.9 (OCH), 61.9 (OCH_2), 34.6 (CH_2), 34.1 (CH_2), 32.4 (CH_2), 32.1 (CH_2), 26.0 (C($\underline{C}H_3$)$_3$), 25.2 (CH_2), 24.8 (CH_2), 23.0 (CH_2), 22.7 (CH_2), 21.1 (CH_3), 17.8 (Si$\underline{C}$(CH_3)$_3$), 16.8 (CH_3), 14.5 (CH_3), 14.3 (CH_3), 14.2 (CH_3), 12.1 (CH_3), 6.9 (3xSi$CH_2\underline{C}H_3$), 5.0 (3xSi$\underline{C}H_2CH_3$), -4.0 ($SiCH_3$), -4.2 ($SiCH_3$).

3.1.9. General Procedure for Steglich Esterification with EDC

At 0 °C, EDC (5 equiv) was added in one portion to a CH_2Cl_2 (4 mL) solution of alcohol (1 equiv), acid (~1.2 eq) and DMAP (4-dimethylaminopyridine, 2 equiv). The reaction was stirred overnight while warming to ambient temperature. At this point, TLC (silica, EtOAc–hexanes) showed the reaction was complete. The reaction mixture was quenched with a few drops of methanol and washed sequentially with 1M HCl and saturated aqueous $NaHCO_3$. The aqueous layers were back extracted with CH_2Cl_2. The combined organic layer was dried over Na_2SO_4 and concentrated under reduced pressure. The residue was purified by column chromatography (silica, EtOAc–hexanes) to give desired compounds.

Analogue **22**: Alcohol **21** (39.6 mg, 0.0411 mmol) was reacted with nonanoic acid **8** (8.0 mg, 0.0506 mmol) to make ester **22**. The crude product was purified by column chromatography (100:1→15:1, hexanes–EtOAc) to afford **22** as a colorless syrup (45.4 mg, contaminated by **8** that could not be separated): R_f 0.70 (6:1 hexanes–EtOAc); ^{1}H NMR (400 MHz, $CDCl_3$, δ_H) 7.59 (d, *J* = 16.0 Hz, 1H), 7.43–7.52 (m, 2H), 7.32–7.40 (m, 3H), 6.79 (br q, *J* = 6.0 Hz, 1H), 6.31 (d, *J* = 16.0 Hz, 1H), 5.23 (t, *J* = 8.9 Hz, 1H), 5.09 (t, *J* = 9.8 Hz, 1H), 4.96–5.03 (m, 2H), 4.31 (d, *J* = 7.7 Hz, 1H), 4.17 (d, *J* = 4.0 Hz, 2H), 4.04 (d, *J* = 8.4 Hz, 1H), 3.89 (dd, *J* = 9.2, 3.6 Hz, 1H), 3.50–3.70 (m, 4H), 2.33 (t, *J* = 7.4 Hz, 2H), 2.11 (s, 3H), 1.68–1.78 (m, 6H), 1.17–1.66 (m, 28H), 1.13 (d, *J* = 6.4 Hz, 3H), 0.80–1.01 (m, 27H), 0.46–0.66 (m, 6H), 0.18 (s, 3H), 0.12 (s, 3H); ^{13}C NMR (100 MHz, $CDCl_3$, δ_C) 173.5 (C=O), 171.0 (C=O), 167.0 (C=O), 165.6 (C=O), 146.0 (=CH), 138.1 (=CH), 134.2 (=C), 130.6 (=CH), 128.9 (2x=CH), 128.3 (2x=CH), 128.2 (=C), 117.0 (=CH), 101.3 (O_2CH), 100.6 (O_2CH), 81.7 (OCH), 75.3 (OCH), 74.5 (OCH), 74.3 (OCH), 74.1 (OCH), 73.6 (OCH), 71.8 (OCH), 69.6 (OCH), 68.8 (OCH), 62.9(OCH_2), 34.7 (CH_2), 34.2 (CH_2), 34.1 (CH_2), 32.5 (CH_2), 32.1 (CH_2), 31.9 (CH_2), 26.0 (C($\underline{C}H_3$)$_3$), 29.3 (CH_2), 29.2 (CH_2), 29.1 (CH_2), 25.3 (CH_2), 24.8(1) (CH_2), 24.7(7) (CH_2), 23.0 (CH_2), 22.7(5) (CH_2), 22.7(2) (CH_2), 21.1 (CH_3), 17.9 (Si$\underline{C}$(CH_3)$_3$), 16.8 (CH_3), 14.5 (CH_3), 14.4 (CH_3), 14.2 (2xCH_3), 12.1 (CH_3), 6.9 (3xSi$CH_2\underline{C}H_3$), 5.0 (3xSi$\underline{C}H_2CH_3$), -4.1 ($SiCH_3$), -4.2 ($SiCH_3$).

Analogue **23**: Alcohol **21** (39.1 mg, 0.0406 mmol) was reacted with acid **9** (10.6 mg, 0.0566 mmol) to make ester **23**. The crude product was purified by column chromatography (50:1→10:1, hexanes–EtOAc) to afford **23** as a colorless syrup (46.0 mg, quantitative). The ratio of the two rotamers (~3:1) was estimated from the ^{13}C NMR spectrum. ^{1}H NMR and ^{13}C NMR are reported for the major rotamer: R_f 0.36 (3:1 hexanes–EtOAc); ^{1}H NMR (400 MHz, $CDCl_3$, δ_H) 7.57 (d, *J* = 16.0 Hz, 1H), 7.42–7.51 (m, 2H), 7.31–7.39 (m, 3H), 6.77 (q, *J* = 7.0 Hz, 1H), 6.29 (d, *J* = 16.0 Hz, 1H), 4.95–5.30 (m, 4H), 4.22–4.43 (m, 3H), 4.07–4.19 (m, 1H), 3.82–4.06 (m, 3H), 3.45–3.72 (m, 4H), 3.04 (s, 3H), 2.33 (t, *J* = 7.5 Hz, 2H), 2.10 (s, 3H), 1.66–1.76 (m, 6H), 1.17–1.66 (m, 22H), 1.11 (d, *J* = 6.4 Hz, 3H), 0.80–1.01 (m, 27H), 0.45–0.64 (m, 6H), 0.17 (s, 3H), 0.10 (s, 3H); ^{13}C NMR (100 MHz, $CDCl_3$, δ_C) 174.0 (C=O), 170.9 (C=O), 169.1 (C=O), 166.9 (C=O), 165.7 (C=O), 146.2 (=CH), 138.2 (=CH), 134.2 (=C), 130.6 (=CH), 129.0 (2x=CH), 128.4 (2x=CH), 128.2 (=C), 116.9 (=CH), 101.4 (O_2CH), 100.6 (O_2CH), 81.8 (OCH), 75.1 (OCH), 74.5 (OCH), 74.4 (OCH), 74.0 (OCH), 73.6 (OCH), 71.7 (OCH), 69.6 (OCH), 68.8 (OCH), 61.5(OCH_2), 48.9 (NCH_2), 36.5 (CH_3), 34.7 (CH_2), 34.2 (CH_2), 33.2 (CH_2), 32.5 (CH_2), 32.1 (CH_2), 31.6 (CH_2), 26.0

 doi:10.20944/preprints202410.2501.v1

(C(CH$_3$)$_3$), 25.2 (CH$_2$), 24.8 (CH$_2$), 24.6 (CH$_2$), 23.0 (CH$_2$), 22.8 (CH$_2$), 22.6 (CH$_2$), 21.1 (CH$_3$), 17.9 (SiC(CH$_3$)$_3$), 16.8 (CH$_3$), 14.5 (CH$_3$), 14.4 (CH$_3$), 14.2 (CH$_3$), 14.1 (CH$_3$), 12.1 (CH$_3$), 6.9 (3xSiCH$_2$CH$_3$), 6.9 (3xSiCH$_2$CH$_3$), -4.0 (SiCH$_3$), -4.2 (SiCH$_3$).

3.1.10. General Procedure for TES and TBS Removal Using TBAF/AcOH

To a solution of TES and TBS protected compounds (1 equiv) in THF (2 mL) was added AcOH (37 equiv) and TBAF (1M solution in THF, 22 equiv) at room temperature. The reaction was then stirred at room temperature for 8 h. At this point, TLC (silica, EtOAc–hexanes) showed the reaction was complete. The reaction mixture was diluted with CH_2Cl_2 and washed sequentially with 1M HCl, saturated aqueous $NaHCO_3$ and brine. The aqueous layers were back extracted with CH_2Cl_2. The combined organic layer was dried over Na_2SO_4 and concentrated under reduced pressure. The residue was purified by column chromatography (silica, EtOAc–hexanes) to give desired analogues.

Analogue **10**: The TES and TBS groups in **22** (45.4 mg, 0.0411 mmol) were removed by TBAF/AcOH. The crude product was purified by column chromatography (15:1→2:1, hexanes–EtOAc) to afford **11** as a colorless to pale yellow syrup (29.8 mg, 83%): R_f 0.55 (1:1 hexanes–EtOAc); ^{1}H NMR (400 MHz, $CDCl_3$, δ_H) 7.57 (d, *J* = 16.0 Hz, 1H), 7.38–7.48 (m, 2H), 7.26–7.38 (m, 3H), 6.75–6.87 (m, 1H), 6.27 (d, *J* = 16.0 Hz, 1H), 5.10–5.26 (m, 3H), 4.65 (d, *J* = 8.2 Hz, 1H), 4.38 (d, *J* = 7.3 Hz, 1H), 4.24 (br s, 1H), 4.13 (d, *J* = 3.8 Hz, 2H), 3.55–3.84 (m, 7H), 2.24 (td, *J* = 7.6, 3.2 Hz, 2H), 2.14 (s, 3H), 1.63–1.76 (m, 6H), 1.36–1.55 (m, 6H), 1.14–1.35 (m, 22H), 1.12 (d, *J* = 6.4 Hz, 3H), 0.73–0.88 (m, 9H); ^{13}C NMR (100 MHz, $CDCl_3$, δ_C) 173.6 (C=O), 171.4 (C=O), 168.1 (C=O), 165.6 (C=O), 146.6 (=CH), 139.2 (=CH), 134.1 (=C), 130.8 (=CH), 129.0 (2x=CH), 128.4 (2x=CH), 127.8 (=C), 116.6 (=CH), 102.8 (O$_2$CH), 99.6 (O$_2$CH), 79.3 (OCH), 77.7 (OCH), 74.4 (OCH), 72.8 (OCH), 72.2 (OCH), 71.8 (OCH), 70.8 (OCH), 69.3 (OCH), 68.3 (OCH), 62.3 (OCH$_2$), 34.4 (CH$_2$), 34.0 (CH$_2$), 33.4 (CH$_2$), 32.1 (CH$_2$), 31.9 (2xCH$_2$), 29.3 (CH$_2$), 29.2(4) (CH$_2$), 29.2(2) (CH$_2$), 24.7(9) (CH$_2$), 24.7(7) (2xCH$_2$), 24.7(4) (CH$_2$), 22.7(1) (CH$_2$), 22.6(8) (CH$_2$), 21.1 (CH$_3$), 16.4 (CH$_3$), 14.6 (CH$_3$), 14.2(0) (2xCH$_3$), 14.1(7) (CH$_3$), 12.1 (CH$_3$). HRMS *m/z* calcd for $C_{48}H_{74}NaO_{14}$ $[M+Na]^+$ 897.4969, found: 897.4976. Purity: 95.4% (MeCN/H_2O 97:3; 1.5 mL/min, t_R = 14.336 min).

Analogue **11**: The TES and TBS groups in **23** (46.0 mg, 0.0406 mmol) were removed by TBAF/AcOH. The crude product was purified by column chromatography (10:1→1:1, hexanes–EtOAc) to afford **11** as a colorless to pale yellow syrup (31.6 mg, 86%). The ratio of the two rotamers (~4:1) was estimated from the ^{13}C NMR spectrum. ^{1}H NMR and ^{13}C NMR are reported for the major rotamer: R_f 0.57 (1:2 hexanes–EtOAc); ^{1}H NMR (400 MHz, $CDCl_3$, δ_H) 7.61 (d, *J* = 16.0 Hz, 1H), 7.44–7.52 (m, 2H), 7.32–7.41 (m, 3H), 6.78–6.88 (m, 1H), 6.31 (d, *J* = 16.0 Hz, 1H), 5.11–5.31 (m, 3H), 4.70 (d, *J* = 8.2 Hz, 1H), 4.38 (d, *J* = 6.7 Hz, 1H), 4.22–4.31 (m, 3H), 3.98 (d, *J* = 17.4 Hz, 1H), 3.61–3.90 (m, 8H), 3.03 (s, 3H), 2.33 (t, *J* = 7.4 Hz, 2H), 2.18 (s, 3H), 1.66–1.78 (m, 6H), 1.40–1.66 (m, 6H), 1.18–1.36 (m, 16H), 1.16 (d, *J* = 6.4 Hz, 3H), 0.78–0.90 (m, 9H); ^{13}C NMR (100 MHz, $CDCl_3$, δ_C) 174.1 (C=O), 171.4 (C=O), 169.3 (C=O), 167.9 (C=O), 165.7 (C=O), 146.7 (=CH), 139.0 (=CH), 134.0 (=C), 130.8 (=CH), 129.1 (2x=CH), 128.4 (2x=CH), 127.9 (=C), 116.5 (=CH), 102.5 (O$_2$CH), 99.6 (O$_2$CH), 79.3 (OCH), 77.3 (OCH), 74.2 (OCH), 72.7 (OCH), 72.2 (OCH), 71.8 (OCH), 70.7 (OCH), 69.3 (OCH), 68.3 (OCH), 62.8 (OCH$_2$), 49.2 (NCH$_2$), 36.5 (CH$_3$), 34.4 (CH$_2$), 33.5 (CH$_2$), 33.2 (CH$_2$), 32.0 (CH$_2$), 31.9 (CH$_2$), 31.6 (CH$_2$), 24.8 (2xCH$_2$), 24.6 (CH$_2$), 22.7 (2xCH$_2$), 22.6 (CH$_2$), 21.1 (CH$_3$), 16.4 (CH$_3$), 14.6 (CH$_3$), 14.1(8) (CH$_3$), 14.1(5) (CH$_3$), 14.0(6) (CH$_3$), 12.1 (CH$_3$). HRMS *m/z* calcd for $C_{48}H_{73}NNaO_{15}$ $[M+Na]^+$ 926.4871, found: 926.4878. Purity: 95.1% (MeCN/H_2O 87:13; 1.0 mL/min, t_R = 17.144 min).

3.2. Biological Analysis

3.2.1. Cell Culture

The MDA-MB-231 breast cancer cell line was maintained in a DMEM/HIGH culture medium supplemented with 10% fetal bovine serum (FBS) and 2 mM L-glutamine, so-called complete medium. Cell cultures were grown in monolayers in a humidified atmosphere of 5% CO_2 and 95% air at 37 ºC. The culture medium was changed every 2–4 days based on confluency. Once confluent, cell cultures were passaged once or twice a week using trypsin-EDTA (0.05–0.1%) to detach the cells

 doi:10.20944/preprints202410.2501.v1

from their culture dishes. Cell images were taken using an Invitrogen EVOS XL Core Imaging System (AMEX 1000).

3.2.2. AlamarBlue Viability Assays

Counting of viable cells was performed before each experiment. Experiments were done in duplicate or triplicate. First, 75 µL of cell suspension at the density of 40,000 cells/mL was seeded in a 96-well plate (3,000 cells/well), which was incubated at 37 ºC in 5% CO_2 for 24 hours. The compounds were dissolved in DMSO (dimethyl sulfoxide) to make drug stocks (10 mM). The stock solutions were diluted with the complete DMEM/HIGH medium supplemented with penicillin and streptomycin to make a series of gradient fresh working solutions right before each test. The highest amount of DMSO was controlled to be lower than 0.5%. Subsequently, the cells were treated with 75 µL of the freshly made gradient working solution in the total volume of 150 µL/well for 72 hours. After that, 15 µL of alamarBlue stock solution was added to each well. The plate was then incubated at 37 ºC in 5% CO_2 atmosphere for another 1–3 hours and the emission of each well at 590 nm was detected using a Synergy H1 Hybrid multi-mode plate reader (BioTek, Agilent) at excitation 560 nm.

The percentage viability compared to the negative control (DMSO-treated cells as the 100% scale) and the blank control (medium only without cells as the 0% scale) was determined and Prism 6 (GraphPad) used to make a plot of viability (%) versus sample concentration and to calculate the concentration at which each compound exhibited 50% inhibition. EC_{50} value estimates were determined using nonlinear regression to fit data between the top and bottom plateaus to a curve of variable slope (four parameters) using the least-squares fitting method. Absolute IC_{50} value estimates were determined using nonlinear regression to fit normalized data between 100% and 0% to a curve of variable slope using the least-squares fitting method.

4. Conclusions

Inspired by the lately discovered structural information on small molecule-bound Sec61α [27], we designed two new open-chain analogues (**10** and **11**) of Ipom-F to explore the role of the carbonyl group at C-4 of the fatty acid chain. Both molecules were synthesized successfully and assayed for their ability to inhibit growth of MDA-MB-231 breast cancer cells. After scrutinizing the SAR information derived from the new as well as some related previous analogues (**1** and **3**–**6**), we conclude that the carbonyl group possesses two functional roles. As revealed by the Cryo-EM structure, the carbonyl oxygen forms polar interactions (most likely hydrogen bonding) with N300 in Sec61α. More importantly, we believe that this polar functional group with a sp^2 hybridized carbon would disfavor unnecessarily strong interactions with membrane lipids in the lateral gate that may alter overall molecular conformation, therefore reducing binding affinity to the protein. Contributions of these two functional roles to the overall binding of an Ipom-F derivative to Sec61α vary, depending on other parts of the molecule, e.g. cyclic vs. acyclic. Moreover, the work presented here opens a new avenue for future exploration of novel ring-opened Ipom-F analogues containing amino acids/peptides.

Supplementary Materials: The following supporting information can be downloaded at the website of this paper posted on Preprints.org, Supporting information 1: Chemical syntheses and NMR characterization of carboxylic acid building block **9**; Supporting information 2: 1D (^{1}H and ^{13}C) and/or 2D (COSY, HMQC, and/or HMBC) NMR spectra for compounds **10, 11, 15, 16, 17, 18, 21, 22** and **23**.

Author Contributions: Conceptualization, W.Q.S.; methodology, A.K., P.N., A.M. and K.S.; formal analysis, A.K. and W.Q.S.; investigation, A.K., P.N., A.M. and K.S. and W.Q.S.; resources, R.E.S; writing—original draft preparation, A.K. and W.Q.S.; writing—review and editing, A.K., P.N., A.M., K.S., R.E.S . and W.Q.S.; supervision, R.E.S. and W.Q.S.; project administration, W.Q.S.; funding acquisition, W.Q.S. All authors have read and agreed to the published version of the manuscript.

Funding: This work was funded by an AREA grant GM116032 from the National Institute of General Medical Sciences of the National Institutes of Health (NIH) and the start-up funds from Ball State University (W.Q.S.).

Institutional Review Board Statement: Not applicable.

Informed Consent Statement: Not applicable.

Data Availability Statement: Data is contained within the article or supplementary material.

Acknowledgments: Not applicable.

Conflicts of Interest: The authors declare no conflict of interest. The funders had no role in the design of the study; in the collection, analyses, or interpretation of data; in the writing of the manuscript, or in the decision to publish the results.

Sample Availability: Samples of the final compounds (Ipom-F, **3**, **10** and **11**) are available from the authors.

Abbreviations Used: AcOH, acetic acid; CMPI, 2-chloro-1-methylpyridinium iodide; cryo-EM, cryogenic electron microscopy; DCC, *N*,*N*′-dicyclohexylcarbodiimide; DCM, dichloromethane; DMAP, 4-dimethylaminopyridine; DMSO, dimethyl sulfoxide; EC_{50}, half-maximal effective concentration; EDC, 1-ethyl-3-(3-dimethylaminopropyl)carbodiimide); equiv, equivalent; ER, endoplasmic reticulum; EtOAc, ethyl acetate; HCT-116, human colorectal cancer cells; HRMS, High resolution mass spectrometry; IC_{50}, half-maximal inhibitory concentration; Ipom-F, ipomoeassin F; MDA-MB-231, human epithelial breast cancer cells; Lev, levulinoyl; N300, asparagine-300; NCI, National Cancer Institute; SAR, structure–activity relationship; Sec61α, alpha subunit of the Sec61 complex; TBAF, tetra-n-butylammonium fluoride; TBS, *tert*-butyldimethylsilyl; TEA, triethylamine; TES, triethylsilyl; TESOTf, triethylsilyl triflate; TFA, trifluoroacetic acid; TLC, thin-layer chromatography; TMSOTf, trimethylsilyl triflate.

References

1. Newman, D.J.; Cragg, G.M. Natural Products as Sources of New Drugs over the Nearly Four Decades from 01/1981 to 09/2019. *J. Nat. Prod.* **2020**, *83*, 770-803, doi:10.1021/acs.jnatprod.9b01285.
2. Luesch, H.; Paavilainen, V.O. Natural products as modulators of eukaryotic protein secretion. *Nat. Prod. Rep.* **2020**, *37*, 717-736, doi:10.1039/C9NP00066F.
3. Pauwels, E.; Schülein, R.; Vermeire, K. Inhibitors of the Sec61 Complex and Novel High Throughput Screening Strategies to Target the Protein Translocation Pathway. *Int. J. Mol. Sci.* **2021**, *22*, 12007.
4. Osborne, A.R.; Rapoport, T.A.; Berg, B.v.d. PROTEIN TRANSLOCATION BY THE SEC61/SECY CHANNEL. *Annu. Rev. Cell Dev. Biol.* **2005**, *21*, 529-550, doi:10.1146/annurev.cellbio.21.012704.133214.
5. Lang, S.; Pfeffer, S.; Lee, P.-H.; Cavalié, A.; Helms, V.; Förster, F.; Zimmermann, R. An Update on Sec61 Channel Functions, Mechanisms, and Related Diseases. *Front. Physiol.* **2017**, *8*, doi:10.3389/fphys.2017.00887.
6. O'Keefe, S.; Pool, M.R.; High, S. Membrane protein biogenesis at the ER: the highways and byways. *FEBS J.* **2022**, *289*, 6835-6862, doi:10.1111/febs.15905.
7. Garrison, J.L.; Kunkel, E.J.; Hegde, R.S.; Taunton, J. A substrate-specific inhibitor of protein translocation into the endoplasmic reticulum. *Nature* **2005**, *436*, 285, doi:10.1038/nature03821.
8. Tranter, D.; Paatero, A.O.; Kawaguchi, S.; Kazemi, S.; Serrill, J.D.; Kellosalo, J.; Vogel, W.K.; Richter, U.; Mattos, D.R.; Wan, X.; et al. Coibamide A Targets Sec61 to Prevent Biogenesis of Secretory and Membrane Proteins. *ACS Chem. Biol.* **2020**, *15*, 2125-2136, doi:10.1021/acschembio.0c00325.
9. Junne, T.; Wong, J.; Studer, C.; Aust, T.; Bauer, B.W.; Beibel, M.; Bhullar, B.; Bruccoleri, R.; Eichenberger, J.; Estoppey, D.; et al. Decatransin, a new natural product inhibiting protein translocation at the Sec61/SecYEG translocon. *J. Cell Sci.* **2015**, *128*, 1217-1229, doi:10.1242/jcs.165746.
10. Hall, B.S.; Hill, K.; McKenna, M.; Ogbechi, J.; High, S.; Willis, A.E.; Simmonds, R.E. The Pathogenic Mechanism of the Mycobacterium ulcerans Virulence Factor, Mycolactone, Depends on Blockade of Protein Translocation into the ER. *PLoS Pathog.* **2014**, *10*, doi:10.1371/journal.ppat.1004061.
11. McKenna, M.; Simmonds, R.E.; High, S. Mechanistic insights into the inhibition of Sec61-dependent co- and post-translational translocation by mycolactone. *J. Cell Sci.* **2016**, *129*, 1404-1415, doi:10.1242/jcs.182352.
12. Liu, Y.; Law, B.K.; Luesch, H. Apratoxin A Reversibly Inhibits the Secretory Pathway by Preventing Cotranslational Translocation. *Mol. Pharmacol.* **2009**, *76*, 91-104, doi:10.1124/mol.109.056085.
13. Paatero, Anja O.; Kellosalo, J.; Dunyak, Bryan M.; Almaliti, J.; Gestwicki, Jason E.; Gerwick, William H.; Taunton, J.; Paavilainen, Ville O. Apratoxin Kills Cells by Direct Blockade of the Sec61 Protein Translocation Channel. *Cell Chem. Biol.* **2016**, *23*, 561-566, doi:10.1016/j.chembiol.2016.04.008.
14. Zong, G.; Hu, Z.; O'Keefe, S.; Tranter, D.; Iannotti, M.J.; Baron, L.; Hall, B.; Corfield, K.; Paatero, A.O.; Henderson, M.J.; et al. Ipomoeassin F Binds Sec61α to Inhibit Protein Translocation. *J. Am. Chem. Soc.* **2019**, *141*, 8450-8461, doi:10.1021/jacs.8b13506.
15. Cao, S.; Norris, A.; Wisse, J.H.; Miller, J.S.; Evans, R.; Kingston, D.G.I. Ipomoeassin F, a new cytotoxic macrocyclic glycoresin from the leaves of Ipomoea squamosa from the Suriname rainforest. *Nat. Prod. Res.* **2007**, *21*, 872-876, doi:10.1080/14786410600929576.
16. Postema, M.H.D.; TenDyke, K.; Cutter, J.; Kuznetsov, G.; Xu, Q. Total Synthesis of Ipomoeassin F. *Org. Lett.* **2009**, *11*, 1417-1420.

17. Nagano, T.; Pospíšil, J.; Chollet, G.; Schulthoff, S.; Hickmann, V.; Moulin, E.; Herrmann, J.; Müller, R.; Fürstner, A. Total Synthesis and Biological Evaluation of the Cytotoxic Resin Glycosides Ipomoeassin A–F and Analogues. *Chem. Eur. J.* **2009**, *15*, 9697-9706.
18. Zong, G.; Barber, E.; Aljewari, H.; Zhou, J.; Hu, Z.; Du, Y.; Shi, W.Q. Total Synthesis and Biological Evaluation of Ipomoeassin F and Its Unnatural 11R-Epimer. *J. Org. Chem.* **2015**, *80*, 9279-9291, doi:10.1021/acs.joc.5b01765.
19. Zong, G.; Aljewari, H.; Hu, Z.; Shi, W.Q. Revealing the Pharmacophore of Ipomoeassin F through Molecular Editing. *Org. Lett.* **2016**, *18*, 1674-1677, doi:10.1021/acs.orglett.6b00555.
20. Zong, G.; Whisenhunt, L.; Hu, Z.; Shi, W.Q. Synergistic Contribution of Tiglate and Cinnamate to Cytotoxicity of Ipomoeassin F. *J. Org. Chem.* **2017**, *82*, 4977-4985, doi:10.1021/acs.joc.7b00409.
21. Zong, G.; Hirsch, M.; Mondrik, C.; Hu, Z.; Shi, W.Q. Design, synthesis and biological evaluation of fucose-truncated monosaccharide analogues of ipomoeassin F. *Bioorg. Med. Chem. Lett.* **2017**, *27*, 2752-2756, doi:10.1016/j.bmcl.2017.04.065.
22. Zong, G.; Hu, Z.; Duah, K.B.; Andrews, L.E.; Zhou, J.; O'Keefe, S.; Whisenhunt, L.; Shim, J.S.; Du, Y.; High, S.; et al. Ring Expansion Leads to a More Potent Analogue of Ipomoeassin F. *J. Org. Chem.* **2020**, *85*, 16226-16235, doi:10.1021/acs.joc.0c01659.
23. O'Keefe, S.; Roboti, P.; Duah, K.B.; Zong, G.; Schneider, H.; Shi, W.Q.; High, S. Ipomoeassin-F inhibits the in vitro biogenesis of the SARS-CoV-2 spike protein and its host cell membrane receptor. *J. Cell Sci.* **2021**, *134*, doi:10.1242/jcs.257758.
24. Tao, S.; Yang, E.J.; Zong, G.; Mou, P.K.; Ren, G.; Pu, Y.; Chen, L.; Kwon, H.J.; Zhou, J.; Hu, Z.; et al. ER translocon inhibitor ipomoeassin F inhibits triple-negative breast cancer growth via blocking ER molecular chaperones. *Int. J. Biol. Sci.* **2023**, *19*, 4020-4035, doi:10.7150/ijbs.82012.
25. Hau, A.M.; Greenwood, J.A.; Löhr, C.V.; Serrill, J.D.; Proteau, P.J.; Ganley, I.G.; McPhail, K.L.; Ishmael, J.E. Coibamide A Induces mTOR-Independent Autophagy and Cell Death in Human Glioblastoma Cells. *PLOS One* **2013**, *8*, e65250, doi:10.1371/journal.pone.0065250.
26. O'Keefe, S.; Bhadra, P.; Duah, K.B.; Zong, G.; Tenay, L.; Andrews, L.; Schneider, H.; Anderson, A.; Hu, Z.; Aljewari, H.S.; et al. Synthesis, Biological Evaluation and Docking Studies of Ring-Opened Analogues of Ipomoeassin F. *Molecules* **2022**, *27*, 4419.
27. Itskanov, S.; Wang, L.; Junne, T.; Sherriff, R.; Xiao, L.; Blanchard, N.; Shi, W.Q.; Forsyth, C.; Hoepfner, D.; Spiess, M.; et al. A common mechanism of Sec61 translocon inhibition by small molecules. *Nat. Chem. Biol.* **2023**, *19*, 1063-1071, doi:10.1038/s41589-023-01337-y.
28. Zong, G.; Sun, X.; Bhakta, R.; Whisenhunt, L.; Hu, Z.; Wang, F.; Shi, W.Q. New insights into structure–activity relationship of ipomoeassin F from its bioisosteric 5-oxa/aza analogues. *Eur. J. Med. Chem.* **2018**, *144*, 751-757, doi:10.1016/j.ejmech.2017.11.022.